



Titre: Development of a MSW gasification model for flexible integration
Title: into a MFA-LCA framework

Auteurs: Geneviève Groleau, Fabrice Tanguay-Rioux, Laurent Spreutels,
Authors: Martin Héroux, & Robert Legros

Date: 2019

Type: Article de revue / Article


Référence: Groleau, G., Tanguay-Rioux, F., Spreutels, L., Héroux, M., & Legros, R. (2019).
Citation: Development of a MSW gasification model for flexible integration into a MFA-LCA
framework. Detritus, 7, 44-54. <https://doi.org/10.31025/2611-4135/2019.13850>

 **Document en libre accès dans PolyPublie**
Open Access document in PolyPublie

URL de PolyPublie:
PolyPublie URL: <https://publications.polymtl.ca/4907/>

Version: Version officielle de l'éditeur / Published version
Révisé par les pairs / Refereed

Conditions d'utilisation: Creative Commons Attribution-Utilisation non commerciale-Pas
Terms of Use: d'oeuvre dérivée 4.0 International / Creative Commons Attribution-
NonCommercial-NoDerivatives 4.0 International (CC BY-NC-ND)

 **Document publié chez l'éditeur officiel**
Document issued by the official publisher

Titre de la revue: Detritus (vol. 7)
Journal Title:

Maison d'édition: Cisa Publisher
Publisher:

URL officiel: <https://doi.org/10.31025/2611-4135/2019.13850>
Official URL:

Mention légale:
Legal notice:

DEVELOPMENT OF A MSW GASIFICATION MODEL FOR FLEXIBLE INTEGRATION INTO A MFA-LCA FRAMEWORK

Geneviève Groleau¹, Fabrice Tanguay-Rioux¹, Laurent Spreutels¹, Martin Héroux² and Robert Legros^{2,*}

¹ *Chaire de Recherche sur la Valorisation des Matières Résiduelles (CRVMR), Chemical Engineering Department, Polytechnique Montreal, Montreal, Canada*

² *Department of Environment, City of Montreal, Montreal, Canada*

Article Info:

Received:
19 November 2018
Revised:
15 August 2019
Accepted:
27 August 2019
Available online:
26 September 2019

Keywords:

MSW
MFA-LCA
Kinetic models
Gasification
Downdraft moving bed
Fluidized bed

ABSTRACT

This paper presents the development of a comprehensive gasification module designed to be integrated in a MFA-LCA framework. From existing gasification models present in the literature, the most appropriate modelling strategy is selected and implemented into the module. This module needs to be able to capture the influence of input parameters, such as gasification reactor type, oxidizing agent, feedstock composition and operating conditions on the process outputs, including syngas yield, its composition and LHV, as well as tar and char contents. A typical gasification process is usually modelled in four steps: drying, pyrolysis, oxidation and reduction. Models representing each of these steps are presented in this paper. Since the type of gasification reactor is taken into account in the module, models for downdraft moving bed and bubbling fluidized bed reactor are also reviewed. The gasification module will be integrated into a MFA framework (VMR-Sys), which enables calculation of relevant gasifier feedstock parameters, such as moisture content, composition, properties and particle size distribution. Outputs from the module will also include elemental compositions obtained from VMR-Sys calculations. Finally, all outputs from the module will be used to build LCA-inventory data.


1. INTRODUCTION

In most developed countries, recyclables have been collected separately for several decades. More recently, source-sorted collections of organics are being implemented, with the aim of recycling this fraction of Municipal Solid Waste (MSW) through anaerobic digestion and composting. Once recyclables and organics are diverted and reintroduced into the circular economy, other recovery loops need to be implemented to deal with the remaining waste stream, often referred to as refuse. At the moment, this stream is mostly disposed of in landfills, but still contains valuable resources (e.g. recyclables and organic wastes) and a potential for energy recovery. Thermochemical treatments, which are characterized by an important waste reduction in mass (70-80%) and in volume (80-90%), appear to be interesting options to recover either resources or energy from the refuse stream (Arena, 2012). More precisely, gasification appears to be particularly well suited to convert a great variety of waste components present in the refuse stream into a quality syngas, appropriate for multiple applications: combined heat and power (CHP), production of valuable chemicals and fuels (Arena, 2012).

Several tools are used in waste management planning to guide decisions. In the past few years, Material Flow Analysis (MFA) gained in popularity as a decision-making tool. MFA models are able to predict output stream characteristics of a given waste treatment process and may be combined with a Life Cycle Assessment (LCA) in order to estimate environmental impacts of a given waste management system. However, since transfer coefficients from empirical data are often used in LCA inventory databases to model material conversions in treatment plants, effects of input stream characteristics and operating conditions are not taken into accounts. In order to capture these effects, a gasification model based on constitutive equations (mass and energy balances, reaction kinetics, transport phenomena) need to be developed. Therefore, the aim of this work is to select the most appropriate modelling strategy in order to develop a comprehensive gasification module designed to be integrated in a MFA-LCA framework.

1.1 Abbreviations and symbols

ABM Agent-Based Model
CHP Combined heat and power

 * Corresponding author:
Robert Legros
email: robert.legros@polymtl.ca

CRVMR	Chaire de Recherche sur la Valorisation des Matières Résiduelles
CSTR	Continuous stirred tank reactor
DST	Decision Making Tool
MSW	Municipal solid waste
LCA	Life cycle assessment
LHV	Lower heating value
PFR	Plug flow reactor
WMS	Waste Management Systems

List of symbols

A_j	Pre-exponential factor of reaction j (1/s)
A_c	Reactor cross sectional area (m^2)
a_c	Particle volumetric surface area (1/m)
C_i	Concentration of component i ($kmol/m^3$)
Cp_i	Specific heat constant of component i ($J/kmol.K$)
D_i	Diffusivity of component i (m^2/s)
d_p	Particle diameter (m)
E_j	Activation energy of reaction j ($J/kmol$)
F_i	Molar flow of component i ($kmol/s$)
f_p	Pyrolysis fraction
k_j	Kinetic rate constant of reaction j (m/s)
k_{m_i}	Mass transfer coefficient of component i (m/s)
L	Reactor length (m)
$\Delta H_{R_{xj}}$	Heat of reaction of reaction j ($J/kmol$)
M	Molecular weight ($kg/kmol$)
m_0	Initial fuel mass (kg)
m_∞	Final fuel mass at $t=\infty$ (kg)
n_i	Number of moles of component i ($kmol$)
r_j	Reaction rate of reaction j ($kmol/m^3s$)
R	Universal gas constant ($J/kmol.K$)
Sh_i	Sherwood number of component i (-)
U_0	Superficial gas velocity (m/s)
U_{mf}	Minimum fluidization velocity (m/s)
U_t	Terminal velocity (m/s)
V	Volume of the reactor (m^3)
X	Extent of conversion (-)
Y_i	Mass fraction of component i (-)

Greek letters

ε	Void fraction (-)
ρ_g	Gas density (kg/m^3)
ρ_s	Solid density (kg/m^3)
τ	Residence time (s)
ν_{ij}	Stoichiometric coefficient of component i in reactions j
ν	Volumetric flow rate (m^3/s)
ν_0	Initial volumetric flow rate (m^3/s)
μ_g	Gas viscosity ($kg/m.s$)
ω	Order of reaction

Subscripts

0	Initial
b	Bed
D	Drying step
g	Gas phase
i	Species
j	Reactions
O	Oxidation step
P	Pyrolysis step

R	Reduction step
s	Solid
T	Total

1.2 Gasification process

During the gasification process, the combustible fraction of MSW is mostly converted into carbon monoxide (CO), hydrogen (H₂) and methane (CH₄) (Arena, 2012). These three gases are the main constituents of syngas. The syngas may also contain vapor, carbon dioxide (CO₂), large amounts of nitrogen (N₂) in the case of air-blown gasifier, and a wide variety of non-desirable components (e.g. H₂S) (Sikarwar et al., 2016). In addition to these gases, solid residues such as char and ash are also formed during gasification, which are both composed of elemental carbon, minerals and metals (Klinghoffer et al., 2011). While char contains mainly elemental carbon, ash is primarily composed of minerals and metals, with minimal elemental carbon (Klinghoffer et al., 2011). Depending on the MSW feedstock, the quality of the syngas may greatly vary (Sikarwar et al., 2017). The effects of MSW moisture content, chemical composition and particle size on the gasifier outlet streams are discussed in the following sections.

1.3 MSW moisture and ash content

MSW components are separated into wet and dry materials, based on their water contents. Dry combustible materials such as plastics, textiles, rubber, leather and wood are characterized by a water content of 0-30%. Wet combustible materials, such as green residues, food and other organic wastes usually contain 40-90% of water. Dry non-combustible materials such as metals, glasses and other inorganic compounds do not contain water and are considered inert (Themelis et al., 2002). The allowable feedstock moisture content depends on the type of reactor. In this study, only downdraft moving bed and bubbling fluidized bed reactors are considered. Downdraft reactor can handle feedstock characterized by less than 20% moisture content, while bubbling fluidized bed reactor feedstock must not exceed 55% moisture content (Arena, 2012). Therefore, in order to meet reactors criteria in terms of moisture content, wet combustible materials should be removed or partially dried before entering the gasification. Finally, the fraction of dry non-combustibles in the feedstock should also be removed prior to the process to reduce its fraction below 20% (Baillie et al., 1997; Themelis et al., 2002; US department of Energy, 2008).

1.4 MSW chemical composition

Since MSW may contain element traces such as sulfur (S) chlorine (Cl) and nitrogen (N), the produced syngas may contain contaminants such as hydrogen sulfide (H₂S), carbonyl sulfide (COS), hydrochloric acid (HCl), ammonia (NH₃) and hydrogen cyanide (HCN) (Sikarwar et al., 2016; US department of Energy, 2008). Furthermore, due to traces of alkali metals in MSW, syngas may also contain traces of sodium (Na) and potassium (K) (Sikarwar et al., 2016). H₂S causes equipment corrosion, while NH₃, HCl and trace

metals contribute to deactivation of catalysts used in the syngas downstream conversion (Sikarwar et al., 2016). MSW feedstock may also contain fluorine (F), arsenic (As) and phosphorus (P), known as catalyst poisons for liquid fuels synthesis processes, as well as volatile metals such as cadmium (Cd) and mercury (Hg, known as potential catalyst poisons and are particularly difficult to remove (US department of Energy, 2008). Finally, the produced syngas from MSW gasification may also contain particulates and tars (Sikarwar et al., 2016). Presence of tars can lead to equipment blockages (Sikarwar et al., 2016). The two types of reactors reviewed in this work, fluidized bed and downdraft moving bed reactors, are selected because of their performance in reducing the amount of tar emitted. In fact, fluidized bed produces tar concentration in syngas of the order of 10 g/m³, while downdraft moving bed reactor produces tar concentration around 1 g/m³ of syngas (Milne et al., 1998; Basu, 2013).

1.5 MSW particle size

Feedstock particle size distribution has direct impacts on the syngas yield (Sikarwar et al., 2016). In fact, with smaller particles, fluid-particle heat transfer is improved and gasification rate is enhanced exponentially (Sikarwar et al., 2016). Higher heat transfer resistance caused by larger particles results in higher residual char yield, due to incomplete pyrolysis (Lv et al., 2004). Finer particles may be elutriated from fluidized beds before complete conversion, thus reducing gasification efficiency and increasing fly ash. In addition a reduction in particle size also increases H₂ yield and decreases tar production (Hernández et al., 2010; Luo et al., 2009; Sikarwar et al., 2016). Therefore, in order to improve the syngas quality, pretreatment including removing or shredding/compacting of large waste articles should be considered before the gasification process (US department of Energy, 2008). Downdraft moving bed reactors can treat particles as large as 50 mm, while fluidized bed reactors usually accept smaller particles of the order of 6 mm (Basu, 2013), although some bubbling fluidized bed reactors have overbed feeding of very large particles.

1.6 Context

The present work aims at developing a comprehensive gasification process module, to be integrated in a Mass Flow Analysis and Life Cycle Assessment (MFA-LCA) framework. The Chaire de Recherche sur la Valorisation des Matières Résiduelles (CRVMR, Research Chair on Advanced Waste Recovery) at Polytechnique Montreal, is currently developing a methodology to assess the sustainability of Waste Management Systems (WMS), based on the integration of three distinct tools:

- VMR-Gen: Agent-Based Model (ABM) to predict the behaviour of the waste generator, providing the MSW flows and compositions of the source-sorted waste streams;
- VMR-Sys: MFA based framework to calculate waste and products flows and stocks throughout the WMS. Comprehensive process modules, one for each waste

treatment technology, are developed and integrated into this framework;

- VMR-Imp: Waste LCA modelling to evaluate the WMS impacts.

The VMR-Sys tool is composed of different process modules (e.g. composting, anaerobic digestion, etc.) all tied together by a MFA calculation framework. Detailed results from VMR-Sys are then used to build the LCA-inventory in VMR-Imp tool. Imbedded in the MFA framework VMR-Sys, the gasification process module will receive detailed information on the feedstock, such as its moisture content, composition and particle size distribution and will capture the influence of a variation of waste flows or compositions for different types of gasification reactors (downdraft moving bed or bubbling fluidized bed). Based on the type of reactor selected, the module will identify the required sets of feedstock properties and thus provide targets for the pretreatment sequence of operations, as shown in Figure 1. The gasification module will then predict the output results in terms of syngas yield, composition and lower heating value (LHV) as well as the composition of tar and char. These outputs will be used in VMR-Imp to build the LCA-inventory data. In order to build a gasification process module, models for each step of the process (drying, pyrolysis, reduction and oxidation) and for the reactor hydrodynamics must be selected. A survey of available modelling strategies is presented in section 2.

2. LITERATURE REVIEW

Typically, gasification processes are separated into four steps: drying, pyrolysis, oxidation and reduction. Figure 2 presents the simplified input and output streams for each step, with their respective chemical compositions. Descriptions of the different modelling approaches for each gasification step and each reactor type are presented in the next sub-sections.

2.1 Gasification process

2.1.1 Drying step

The first step of the gasification process consists of drying. Since the drying characteristic time is considerably shorter than other reaction times in the overall gasification process, this step is often assumed to be instantaneous (Di Blasi, 2000). Stoichiometric relations are the simplest ways to represent the phenomena. In this approach, it is assumed that a fixed fraction of water initially contained in the feedstock is evaporated. The produced vapor is directly added to the other gas components, without the use of kinetic models (Gupta & Bhaskaran, 2018). For example, in the study of Gerber et al. (2010) it is assumed that 10% of the water contained in the feedstock is evaporated.

In order to consider the effects of temperature on the drying yield, kinetically controlled models are used. A typical drying kinetic model is presented in Eq. 1, where r_D , A_D , E_D , T_D and $C_{H_2O(0)}$ represent the evaporation rate (kmol/m³.s), the pre-exponential drying factor (1/s), the activation energy of water evaporation (J/kmol), the drying temperature

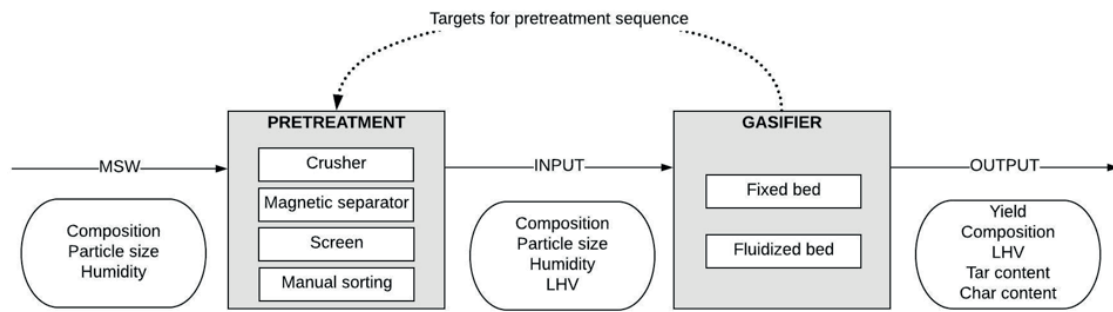


FIGURE 1: Gasification module structure.

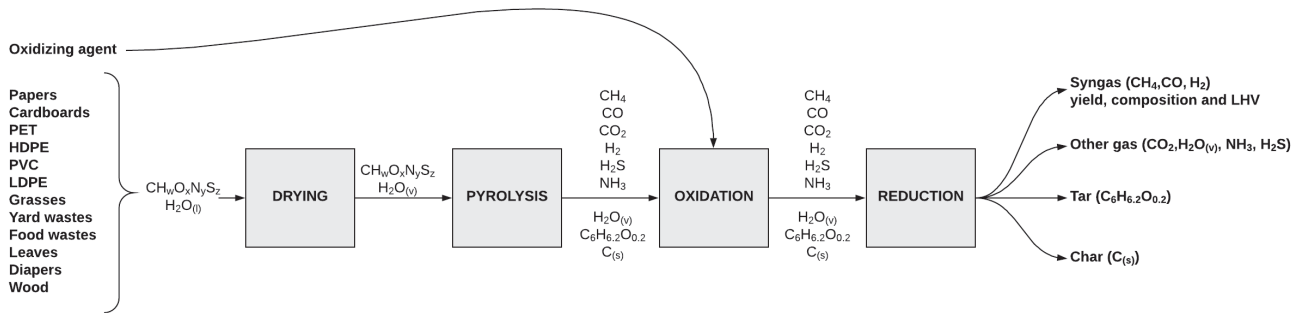


FIGURE 2: Chemical inputs and outputs of the four steps of the gasification process: drying, pyrolysis, oxidation and reduction.

(K) and the water concentration (kmol/m^3), respectively (Salem & Paul, 2018). Constant temperature or a certain temperature profile may be used to describe the drying step. For example, a temperature of 400K is used in the study of Salem & Paul (2018) while a temperature profile ranging from 368K to 473K is used by Dejtrakulwong & Pamtumsawad (2014).

$$r_D = A_D \exp\left(-\frac{E_D}{RT_D}\right) C_{H_2O(l)} \quad (1)$$

Other drying models exist in the literature. For example, in studies by Di Blasi & Branca (2013) and Sharma (2011), a diffusion controlled process is used to describe the drying step. In such models, evaporation rate is limited by vapor diffusion throughout the particle pores (Shokri & Or, 2011). Finally, an isothermal evaporation process is used in a study by Gerber & Oevermann (2014). In this model, the evaporation process is described by a lumped method at a constant evaporation temperature (373K), where a certain amount of water is evaporated over a short time period (Gerber & Oevermann, 2014; Gupta & Bhaskaran, 2018). Since this process is usually very rapid, its kinetic is often neglected.

2.1.2 Pyrolysis step

Once water is partially evaporated, the feedstock is devolatilized into volatiles, tar and char (Sharma, 2011). In the literature, pyrolysis fraction (f_p) and kinetic models are used to describe the mass loss. In the most simplified models, pyrolysis is assumed to occur instantaneously at the feeding location, along with the drying step (Gupta & Bhaskaran, 2018). In a study by Giltrap et al. (2003), the pyrolysis fraction f_p is introduced in order to represent the degree of devolatilization of an instantaneous pyrolysis

process. A f_p of zero indicates no pyrolysis while a f_p of one indicates that feedstock is completely devolatilized into volatiles, tar and char (Giltrap et al., 2003). A f_p of 0.5 is assumed in a study by Giltrap et al. (2003).

Devolatilization process described by a kinetic model is shown in Eq. 2, where m_0 , m_∞ , X and ω represent the feedstock mass at $t=0$ (kg), the feedstock mass at $t=\infty$ (kg), the extent of conversion and the order of reaction, respectively (Grammelis et al., 2009; Gupta & Bhaskaran, 2018). The reaction rate constant is expressed by the Arrhenius reaction rate.

$$-\frac{dm}{dt} = (m_0 - m_\infty) \cdot A_P \exp\left(\frac{-E_P}{RT}\right) (1 - X)^\omega \quad (2)$$

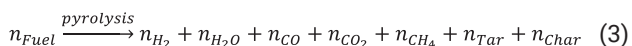
Several pyrolysis kinetic models exist, such as the one-step global model, the one-stage multi-reaction model and the two-stage semi-global model (Gupta & Bhaskaran, 2018; Sheth & Babu, 2006). These pyrolysis models are presented in Table 1, where n represents the number of moles and K_p represents the kinetic rate constant (Di Blasi, 2000; Gupta & Bhaskaran, 2018; Sheth & Babu, 2006). In the one-step global model, pyrolysis is considered as a single-step reaction, where volatiles, tar and char are produced simultaneously (Gupta & Bhaskaran, 2018). On the other hand, in the one-stage multi-reaction model, pyrolysis is represented with several simultaneous competing reactions. Finally, in the two-stage semi-global model, pyrolysis is considered as a two-stage reaction, where the final product (primary tar) of the first reaction produces a secondary tar (Sheth & Babu, 2006).

While pyrolysis fraction f_p and kinetic models predict the mass loss of the solids, other models are used to estimate the volatiles composition (Sharma et al., 2006). In the literature, volatiles usually comprise CO , CO_2 , H_2 , H_2O , CH_4 ,

TABLE 1: Pyrolysis kinetics models used in the gasification process modelling (Babu & Sheth, 2006; Di Blasi, 2000; Gupta & Bhaskaran, 2018).

Models	Equations
One-step global model	$n_{Fuel} \xrightarrow{k_{p1}} n_{volatiles} + n_{Tar} + n_{Char}$
One-stage multi-reactions model	$n_{Fuel} \xrightarrow{k_{p2,1}} n_{volatiles}$
	$n_{Fuel} \xrightarrow{k_{p2,2}} n_{Tar}$
	$n_{Fuel} \xrightarrow{k_{p2,3}} n_{Char}$
Two stage semi-global model	$n_{Fuel} \xrightarrow{k_{p3,1}} n_{volatiles,1} + n_{Tar,1} + n_{Char}$
	$n_{Tar,1} \xrightarrow{k_{p3,2}} n_{volatiles,2} + n_{Tar,2}$

as shown in Eq. 3 (Sharma et al., 2006).



In order to predict pyrolysis product compositions, different methods are used. For example, in a study by Giltrap et al. (2003), an equivalent amount of CO, H₂O and CH₄ was assumed. Other studies use experimental data to estimate the composition. For example, in the work of Di Blasi (2000), experimental data on gasification of wood chips and rice husks are used to estimate the volatiles distribution in terms of CO, CO₂, H₂, H₂O and CH₄.

Other studies such as that by Tinaut et al. (2008) use the method suggested in the work of Thunman et al. (2001), where a set of equations composed of elementary balances and enthalpy balances is solved for the mass fractions of volatile species. Experimental data for ratios of CO/CO₂ and C_xH_y/CO₂ are used to solve the system (Sharma et al., 2006; Thunman et al., 2001).

Finally, in the work of Sharma et al. (2006), a model describing the biomass devolatilization in terms of cellulose, hemicellulose and lignin is used. In order to solve the system of equations composed of elementary balances, experimental ratios of CO/CO₂, H₂O/CO₂ and CH₄/CO₂ are used (Sharma et al., 2006). These ratios are presented in Eq. 4, Eq. 5 and Eq. 6, where represents the mass fraction (Sharma et al., 2006). To close the system of equations, mass fractions of cellulose, hemicellulose and lignin are used as input information to solve for n_{Char}. In the model, it is considered that each of these constituents of dry and ash-free biomass decomposed into a fixed fraction of char and volatiles (Sharma, 2011). Transformation of sulfur (S) and Nitrogen (N) atoms initially contained in the solid are not taken into account in these studies.

$$Y_{CO}/Y_{CO_2} = \exp\left(-1.845 + \frac{7730.3}{T_P} - \frac{5019898}{T_P^2}\right) \quad (4)$$

$$Y_{H_2O}/Y_{CO_2} = 1 \quad (5)$$

$$Y_{CH_4}/Y_{CO_2} = 5 \cdot 10^{-16} \cdot T_P^{5.06} \quad (6)$$

2.1.3 Oxidation step

After the pyrolysis step, volatiles, tar and char are oxidized by reacting with an oxidizing agent (either pure oxygen or air in this work) or with each other (e.g. water-gas shift reaction) (Gupta & Bhaskaran, 2018). The reaction rates of homogeneous reactions and heterogeneous reactions involving char, are presented in Table 2.

In the literature, different approaches are used to predict the oxidation yield. Since all oxidation reaction rates are faster by a few orders of magnitude than those of char reduction reactions, the oxidation step is often assumed to be instantaneous (Babu & Sheth, 2006; Giltrap et al., 2003; Sharma, 2011). For example, in the studies by Giltrap et al.(2003) and Babu & Sheth (2006) an instantaneous and complete oxidation process was assumed at the feeding location.

Other studies, such as the one by Sharma (2011) and Salem & Paul (2018), use a heuristic approach to predict the oxidation yield. In this approach, the oxidation and pyrolysis products are allowed to react with the oxidizing agent available, in a sequence of descending order of reaction rates (Sharma, 2011). Reaction rates listed in Table 2 are only used as a guide to establish the sequence of oxidation reactions described below:

1. Oxidation of hydrogen (reaction O-4)
2. Oxidation of carbon monoxide (reaction O-2)
3. If oxygen remains, the oxidation of methane takes place (reaction O-3)
4. If oxygen still remains, char and tar are oxidized simultaneously according to their reaction rates (reactions O-1 and O-5)

Finally, in studies by Di Blasi & Branca (2013) and Tinaut et al. (2008), kinetic models are used to predict the quantity of gases produced during the oxidation step. Reaction rates presented in Table 2 are used to represent the kinetics of homogeneous reactions (O-2, O-3, O-4, O-5 and WG).

2.1.4 Reduction step

After the oxidation step, the products go through the reduction step in an oxidant-free environment. This step is primarily dominated by heterogeneous reactions, where the char is converted into gaseous products (Gupta & Bhaskaran, 2018). Reactions occurring during the reduction step are presented in Table 3.

These heterogeneous reduction reactions involve the diffusion of a variety of gases (O₂, CO₂, H₂O, H₂) from the bulk gas phase to the outer surface and then into the pores of the char particles (Gupta & Bhaskaran, 2018). As the char reacts, its particle size decreases while its porosity increases, leading to more active sites available for the gas to react and, as a result, to an increase of the extent of reaction (Sharma, 2011). In order to capture these effects, the unreacted shrinking core model, as well as the char reactivity factor model, are used in the literature. The unreacted shrinking core model is described by Eq. 7, where k_p, C_p, a_c and k_{mi} represent the kinetic constant (m/s) of the heterogeneous reactions presented in Table 3, the concentrations (kmol/m³) of the species i (O₂, CO₂, H₂O, H₂), the particle volumetric surface area (1/m) and the mass transfer coefficient (m/s) for the species i, respectively (Di Blasi, 2000).

$$r_j = a_c \frac{c_i}{\left(\frac{1}{k_{mi}}\right) + \left(\frac{1}{k_j}\right)} \quad (7)$$

Equation of the particle volumetric surface area (a_c) is presented in Eq. 8, where ε and d_p represent the bed void-

TABLE 2: Chemical reaction rates in oxidation zone (Sharma, 2011; Tinaut et al., 2008).

Reactions	Reaction rates (mol/m ³ s)
O-1 $C + 0.5O_2 \xrightarrow{k_{O1}} CO$	$r_{O1} = 0.554 \exp\left(-\frac{89\,990}{RT}\right) [C_{O_2}]$
O-2 $CO + 0.5O_2 \xrightarrow{k_{O2}} CO_2$	$r_{O2} = 1.3 \times 10^8 \exp\left(-\frac{166\,280}{RT}\right) [C_{CO}] [C_{O_2}]^{0.25} [C_{H_2O,v}]^{0.5}$
O-3 $CH_4 + 1.5O_2 \xrightarrow{k_{O3}} CO + 2H_2O$	$r_{O3} = 9.2 \times 10^6 \exp\left(-\frac{80\,230}{RT}\right) T [C_{O_2}] [C_{CH_4}]^{0.5}$
O-4 $H_2 + 0.5O_2 \xrightarrow{k_{O4}} H_2O$	$r_{O4} = 1 \times 10^{11} \exp\left(-\frac{42\,000}{RT}\right) [C_{O_2}] [C_{H_2}]$
O-5 $C_6H_{6.2}O_{0.2} + 2.9O_2 \xrightarrow{k_{O5}} 6CO + 3.1H_2$	$r_{O5} = 59.8 \exp\left(-\frac{101\,430}{RT}\right) T^{0.3} [C_{O_2}] [C_{Tar}]^{0.5}$
WG $CO + H_2O \xrightleftharpoons{k_{WG}} CO_2 + H_2$	$r_{WG} = 2.78 \exp\left(-\frac{12\,600}{RT}\right) \left[C_{CO} C_{H_2O,v} - \frac{C_{CO_2} C_{H_2}}{k_{eq}} \right] \quad k_{eq} = 0.0265 \exp\left(-\frac{32\,900}{RT}\right)$

TABLE 3: Chemical reaction rates in reduction zone (Tinaut et al., 2008).

Reactions	Reaction rates (mol/m ³ s) & Reaction rate constants (m/s)
R-1 $C + CO_2 \xrightarrow{k_{R1}} 2CO$	$r_{R1} = a_c \left(\frac{k_{R1} k_{m,CO_2}}{k_{R1} + k_{m,CO_2}} \right) [C_{CO_2}] \quad k_{R1} = (3.42 \cdot T) \exp\left(-\frac{129\,700}{RT}\right)$
R-2 $C + H_2O \xrightarrow{k_{R2}} CO + H_2$	$r_{R2} = a_c \left(\frac{k_{R2} k_{m,H_2O}}{k_{R2} + k_{m,H_2O}} \right) [C_{H_2O}] \quad k_{R2} = 1.67 k_{R1}$
R-3 $C + 2H_2 \xrightarrow{k_{R3}} CH_4$	$r_{R3} = a_c \left(\frac{k_{R3} k_{m,H_2}}{k_{R3} + k_{m,H_2}} \right) [C_{H_2}] \quad k_{R3} = 0.001 \cdot k_{R1}$
R-4 $CH_4 + H_2O \xrightarrow{k_{R4}} CO + 3H_2$	$r_{R4} = 3015 \exp\left(-\frac{125\,520}{RT}\right) [C_{CH_4}] [C_{H_2O,v}]$

age and the particle diameter (m) (Di Blasi, 2000).

$$a_c = \frac{6(1-\varepsilon)}{d_p} \quad (8)$$

The mass transfer coefficient k_{m_i} is defined by Eq. 9, where D_i and Sh_i represent the diffusivity coefficient of species i in the gaseous boundary layer (m²/s) and the Sherwood number obtained from correlation involving Reynold and Schmidt numbers for species i (Fogler, 2016).

$$k_{m_i} = \frac{D_i}{d_p} Sh_i \quad (9)$$

In the literature, a second approach to model heterogeneous reactions consists of the use of a char reactivity factor (CRF). This approach is specifically used in the case of downdraft moving bed gasifier as it directly represents the reactivity of the char along the moving bed (Babu & Sheth, 2006). CRF is used as a multiplier of the pre-exponential factor present in the reaction rates presented in Table 4. In the work of Giltrap et al. (2003), a constant CRF value of 1000 is proposed. In the study by Babu & Sheth (2006), an exponential increment of CRF along the length of the reactor is suggested in order to avoid rapid reaction completion at the beginning of the reduction zone.

2.2 Reactor hydrodynamics

Depending on the number of dimensions being considered, hydrodynamics models can be classified into zero-dimensional, one-dimensional, two-dimensional or three-dimensional models (Basu, 2010). Characteristics of these models are shown in Table 5. In the following sections, selected models are presented for the downdraft moving bed reactor and for the fluidized bed reactor.

2.2.1 Downdraft moving bed reactors

Pressure and temperature profiles exist along the length of downdraft moving bed reactors. In this type of

reactors, the bed pressure drop is proportional to the gas velocity (Levenspiel & Kunii, 2012). Assuming that the reactor operates under steady state conditions and that there is no radial gradients in concentrations, temperature and reaction rates, the downdraft moving bed may be approximated as a plug flow reactor (PFR) (Fogler, 2016). This assumption is mostly valid for large reactors and caution should be applied in the case of small downdraft gasifiers. A few studies, such as those by Di Blasi (2000), Giltrap et al. (2003) and Tinaut et al. (2008), use this type of approximation for downdraft reactors.

2.2.2 Fluidized bed reactors

Fluidized bed reactors are widely used in the industry due to excellent heat and mass transfers, followed by uniform temperature distribution and concentrations throughout the reactor volume (Bandara et al., 2017). It is often considered that the temperature remains constant within the fluidized bed, and that the gas pressure drop across the bed of particles remains constant (Rhodes, 2008).

Since fluidized bed reactors are well mixed, they are often assumed to be analogous to continuous stirred tank reactors (CSTR), resulting in no spatial variation of concentra-

TABLE 4: Reduction reactions used with char reactivity factor (Babu & Sheth, 2006).

Overall reaction rates (mol/m ³ s)
R-1 $r_{R1} = CRF \cdot 3.616 \times 10^4 \exp\left(-\frac{77\,390}{RT}\right) \left[P_{CO_2} - \frac{P_{CO}^2}{k_{eq,1}} \right]$
R-2 $r_{R2} = CRF \cdot 1.517 \times 10^7 \exp\left(-\frac{121\,620}{RT}\right) \left[P_{H_2O} - \frac{P_{CO} P_{H_2}}{k_{eq,2}} \right]$
R-3 $r_{R3} = CRF \cdot 4.189 \exp\left(-\frac{19\,210}{RT}\right) \left[P_{H_2}^2 - \frac{P_{CH_4}}{k_{eq,3}} \right]$
R-4 $r_{R4} = CRF \cdot 73.01 \exp\left(-\frac{36\,150}{RT}\right) \left[P_{CH_4} P_{H_2O} - \frac{P_{CO} P_{H_2}^3}{k_{eq,4}} \right]$

TABLE 5: Hydrodynamic models present in literature (Bandara et al., 2017; Fogler, 2016; Liu et al., 2013).

Models	Characteristics
Zero-dimensional (stirred tank reactor)	Algebraic equations
One-dimensional (plug flow)	Differential equations with respect to volume or catalyst mass
Two-dimensional	Conservation of mass, momentum and energy:
Three-dimensional	<ul style="list-style-type: none"> • Euler-Euler approach: <ul style="list-style-type: none"> - Solid and gas: continuous, Navier-Stokes equation - Transport properties of solids: kinetic theory of granular flow • Eulerian-Lagrange approach: <ul style="list-style-type: none"> - Gas phase: continuous, Navier-Stokes equation - Solid phase: Newtonian equation of motion for each individual particle

tions, temperature and reaction rates (Fogler, 2016). It must be noted that modelling fluidized bed reactors as CSTR may give relatively accurate results, higher precision results usually require complex models that capture more closely the hydrodynamics of such reactors (Fogler, 2016). These effects may be roughly captured by a single-phase PFR model, which considers the gas flowing through the bed in manner similar to a PFR, assuming an average bed voidage, an uniform solid distribution and that high particle mixing and high superficial gas velocities are reached (Mostoufi et al., 2001). Two-phase models are used for higher precision, where the bubbles and the emulsion phases are either represented with CSTR in series, PFR, or with a combination of CSTR and PFR (Jafari et al., 2004). The latter are the most common type of two-phase models used, where the bubble phase is modelled as a PFR and the emulsion phase as a CSTR (Jafari et al., 2004). Other more complex models also exist in the literature, such as three-phase models, capturing the interactions of the bubbles, emulsion and cloud phases (Levenspiel & Kunii, 2012).

3. GASIFICATION MODULE DEVELOPMENT

Keeping with the aim of developing a flexible, yet accurate gasification module capable of capturing the effect of reactor types, simplified models for the drying, pyrolysis, oxidation and reduction steps are selected. Since characteristic times for moisture evaporation, devolatilization and oxidation are considerably shorter than those for char reduction, these processes are often considered to be instantaneous (Di Blasi, 2000). Therefore, stoichiometric relations are used to represent these steps.

3.1 Drying model

An evaporation of 10% of the water initially contained in the MSW is assumed during the drying step. Water content of MSW is provided by VMR-Sys.

3.2 Pyrolysis model

Since the reaction is assumed to be instantaneous and complete, a pyrolysis fraction of 1 is assumed in order to predict the solids mass loss during the pyrolysis step. Therefore, all of the carbon (C), oxygen (O) and hydrogen (H) atoms initially contained in the MSW are transformed into CO, CO₂, CH₄, H₂O_(v), H₂ and char during this step. It is also assumed that the nitrogen (N) and sulfur (S) atoms contained initially in the MSW are transformed into NH₃ and H₂S during this step (Sikarwar et al., 2016).

To take into account the effects of MSW composition, the devolatilization of MSW is described by the breakdown of cellulose, hemicellulose and lignin (Sharma, 2011). The contents of cellulose, hemicellulose and lignin of different MSW components are presented in Table 6. To consider the plastics fraction of the MSW, the feedstock is also separated into HDPE, LDPE, PP, PS, PVC and PET.

Having the MSW composition of plastics, cellulose, hemicellulose and lignin provided by VMR-Sys, the distribution of CO, CO₂, H₂, H₂O, CH₄ is predicted for a certain char yield. In order to predict the amount of char produced, pyrolysis char yields of different plastics and organic fractions of the MSW are used. These fractions are presented in Table 7.

3.3 Oxidation model

Since it is assumed to be instantaneous, a heuristic approach is chosen to describe the reaction sequence during the oxidation step. In this step, the effects of the oxidizing agent type and quantity are taken into account.

3.4 Reduction model

In order to capture the effects of the MSW particle size for both the downdraft reactor and the bubbling fluidized bed reactor in the reduction step, the unreacted shrinking core model is chosen. Particle size distribution is provided by VMR-Sys in order to calculate the overall reaction rate.

3.5 Hydrodynamics models

Keeping with the aim of developing a flexible, yet accurate gasification module capable of capturing the effect of

TABLE 6: Cellulose, hemicellulose and lignin contents (wt.% dry) of organic fraction of MSW (Agarwal et al., 2014; Couhert et al., 2009; Komilis & Ham, 2003; Wang et al., 2015).

	Cellulose	Hemicellulose	Lignin
Papers	64.7	13.0	0.9
Cardboards	59.7	13.8	14.2
Grasses	59.0	38.0	3
Yard wastes	26.82	10.23	24.54
Food wastes	46.09	0.0	12.03
Leaves	9.48	3.24	33.88
Diapers	33.7	4.6	-
Wood	49.8	20.8	26.7

TABLE 7: Pyrolysis char yield (wt%) of different plastics (HDPE, LDPE, PP, PS, PVC, PET) and organic constituents (cellulose, hemicellulose, lignin) (Sharma, 2011; Williams & Williams, 1999).

	HDPE	LDPE	PP	PS	PVC	PET	Cellulose	Hemicellulose	Lignin
Char yield	0	0	0.2	3.5	13.8	15.6	5	10	55

reactor types, simplified reactor models are selected. The downdraft moving bed reactor is modelled as a PFR, while the fluidized bed reactor is approximated as a single-phase model using a CSTR.

3.5.1 Plug flow reactor model

Since the drying, pyrolysis and oxidation steps are assumed to be instantaneous at the feeding location, oxidation products represent the initial molar flows F_{i0} of the reactor (kmol/s). In a PFR, concentrations, temperature, pressure and velocity vary along the reactor length. In order to capture the variation of molar flows along the length, the design equation of the PFR is used. This equation is shown in Eq. 10, where v_{ij} represents the stoichiometric coefficient of species i in reactions j and A_c represents the cross-sectional area of the reactor (m^2) (Fogler, 2016).

$$\frac{dF_i}{dz} = A_c \sum v_{ij} r_{ij} \quad (10)$$

Since gas-phase reactions are present in the reduction zone, concentrations are expressed in terms of temperature and pressure, as shown in Eq. 11 (Fogler, 2016). Having the inlet molar flows (F_{i0}), the entrance volumetric flow rate v_0 (m^3/s) can be obtained.

$$C_i = \frac{F_{i0} F_i P T_0}{v_0 F_T P_0 T} \quad (11)$$

The initial temperature (T_0) and pressure (P_0) for the model are those of the gas coming out of the oxidation zone. Assuming no work and an adiabatic reactor, the temperature profile along the length is described by Eq. 12, where C_{p_i} and $\Delta H_{R_{Xj}}$ represent the mean heat capacity of species i (J/kmol.K) and the heat of reaction of reactions j (J/kmol) (Fogler, 2016).

$$\frac{dT}{dz} = \frac{A_c \sum r_j \Delta H_{R_{Xj}}}{\sum F_i C_{p_i}} \quad (12)$$

The pressure drop across the reduction zone can be evaluated by the Ergun equation, presented in Eq. 13, where μ_g , ρ_g and U_0 represent the gas viscosity (kg/m.s), the gas density (kg/m^3) and the superficial gas velocity (m/s) (Fogler, 2016).

$$\frac{dP}{dz} = 150 \frac{(1-\varepsilon)^2 \mu_g U_0}{\varepsilon^3 d_p^2} + 1.75 \frac{(1-\varepsilon) \rho_g U_0^2}{\varepsilon^3 d_p} \quad (13)$$

The interstitial gas velocity profile (U_g) is expressed in Eq. 14 and the superficial gas velocity profile is shown in Eq. 15 (Di Blasi & Branca, 2013; Rhodes, 2008).

$$\frac{dU_g}{dz} = \frac{1}{\rho_g} \sum_i \sum_j v_{ij} M_i r_{ij} \quad (14)$$

$$\frac{dU_0}{dz} = \varepsilon \frac{dU_g}{dz} \quad (15)$$

Since the char particles shrink during the reduction step, the particle diameter d_p decreases with respect to the char mass loss, as shown in Eq. 16, which assumes spherical particles (Sharma, 2011). Assuming a constant bed voidage and particle density, a decrease in the particle

diameter causes a decrease in the solid velocity (Di Blasi & Branca, 2013). The void fraction is expressed in Eq. 17, where ρ_b and ρ_s represent the bed density (kg/m^3) and the particle density (kg/m^3) (Rhodes, 2008). Finally, the solid velocity profile is presented in Eq. 18, where r_j only takes into account the heterogeneous reactions (Di Blasi & Branca, 2013).

$$d_p = \sqrt[3]{d_{p0}^3 \frac{F_{char}}{F_{char0}}} \quad (16)$$

$$\varepsilon = 1 - \frac{\rho_b}{\rho_s} \quad (17)$$

$$\frac{dU_s}{dz} = -\frac{M_{char}}{\rho} \sum_j r_{jchar} \quad (18)$$

3.5.2 Continuous stirred tank reactor model

The design equation of a CSTR is shown in Eq. 19 (Fogler, 2016). Gas-phase concentrations used in reaction rates are expressed in Eq. 11. The entrance volumetric flow rate v_0 (m^3/s) is assumed to be the volumetric flow rate of the gas produced during the oxidation step, since drying, pyrolysis and oxidation steps are assumed to be instantaneous.

$$V = \frac{F_{i0} - F_i}{-r_i} \quad (19)$$

The initial temperature (T_0) and pressure (P_0) for the model are those of the MSW entering the CSTR. The uniform temperature of the fluidized bed (T) is calculated with Eq. 20, assuming no work and an adiabatic reactor (Fogler, 2016). Since the pressure drop can be approximated as the apparent bed weight, Eq. 21 is used, where L represent the bed height (m) (Rhodes, 2008).

$$T = T_0 + \frac{V \sum r_{ij} \Delta H_{R_{Xij}}}{\sum F_i C_{p_i}} \quad (20)$$

$$\Delta P = L(1 - \varepsilon)(\rho_s - \rho_g)g \quad (21)$$

Assuming a constant bed voidage and particle density, particle shrinkage causes a decrease in the solid velocity (Di Blasi & Branca, 2013). In order to calculate the particle diameter and the bed voidage, Eq. 16 and Eq. 17 are used (Rhodes, 2008; Sharma, 2011). In order to predict the residence time of the MSW in both gasifiers, Eq. 22 is used, where τ represents the residence time (s) (Fogler, 2016).

$$\tau = \frac{V}{v_0} \quad (22)$$

3.6 Elements partitioning

In order to complete the mass balance for the gasification process, all non-reactive elements must be partitioned between the outlet gas and solids streams. This is achieved by partitioning the non-reactive elements that are tracked by the VMR-Sys using coefficients obtained from different studies. A compilation of these partitioning hypotheses is presented in Table 8.

TABLE 8: Partitioning of non-reactive elements (Arena & Di Gregorio, 2013; Clarke & Sloss, 1992; Gupta & Bhaskaran, 2018; Jung et al., 2005; Kamińska-Pietrzak & Smoliński, 2013; Tanigaki & Ishida, 2014; Vejehati, et al., 2010; Wilk et al., 2011).

	Group 1	Group 1-2	Group 2	Group 2-3	Group 3
Elements	Fe, K, Mn, Al	Ba, Be, Co, Cr, Cu, Mo, Ni,	As, Ca, Na, P, Pb, S, Si, Sn, Ti, Zn	B, Se	Br, Hg, I, F, Cl, N
Hypothesis	0.25: Fly Ash 0.75: Bottom Ash	0.5: Fly Ash 0.5: Bottom Ash	0.75: Fly Ash 0.25: Bottom Ash	0.5: Fly Ash 0.5: Gas	1: Gas

4. VALIDATION OF THE GASIFICATION MODULE PREDICTIONS

The predictions obtained with the gasification module are validated with the syngas compositions of CO, N₂, H₂, CH₄ and CO₂ presented in two experimental studies: 1. Jayah et al. (2003), with wood as feedstock; 2. Garcia-Bacaicoa et al. (2008), with a mixture of wood and HDPE as feedstock. Both studies were carried out in pilot scale fixed beds operating under a co-current mode. Characteristics of these flows and the operating conditions are presented in Table 9.

Predicted syngas composition from the module are presented in Figure 3 for the two experimental sets of conditions. It can be seen that the predictions agree generally well with results obtained in the two experimental studies. For the comparison with the experimental results from by Jayah et al., (2003), the elementary compositions in terms of C, H, O, N, S and volatile materials, fixed carbon, ash and wood moisture content presented in their work were used. It is possible to observe good agreement between the module predictions and the experimental results for CO₂, CH₄ and CO, while larger amounts of H₂ are predicted.

With regard to comparison between the module predictions and the experimental results presented in the work of Garcia-Bacaicoa et al., (2008), where the feedstock was composed of wood mixed with HDPE, the elementary compositions were determined using data provided by VMR-Sys since they were not provided by the authors. This enabled a first validation of the integration between the gasification

module and the MFA-LCA framework. The results are very encouraging as seen in Figure 3. However, looking at the data presented in Figure 3, it is possible to see that the module predicts larger amounts of H₂ and CO₂ and lower amounts of CO. This could be attributed to the fact that the elementary compositions describing wood and HDPE provided by VMR-Sys might be slightly different from the actual elementary compositions of the feedstocks used in this study.

In regard to the larger quantities of H₂ predicted by the module compared with the experimental results, this may be explained by the limitations associated with the Water-Gas Shift (WGS) reaction in the reduction zone to adequately predicts the balance of CO, CO₂, H₂O and H₂. Since the WGS reaction is characterized by slow reaction kinetics, very little H₂ and CO₂ are converted into CO and H₂O. These effects therefore slightly increase the H₂/CO ratio and reduce the H₂/CO/CO₂ ratio of the syngas produced. However, given the general consistency of the module predictions with the two experimental studies used for data validation, it is reasonable to conclude that the developed gasification module offers a very useful tool to be integrated in a MFA-LCA framework since it is able to capture the influence of feedstock composition and properties, together with the operating conditions of the gasifier.

5. CONCLUSIONS

In order to develop a comprehensive gasification process module to be integrated in a MFA-LCA framework, a review of available models was presented. The gasification process was divided into four steps: drying, pyrolysis, oxidation and reduction. Drying, pyrolysis and oxidation are assumed to be instantaneous. Four models representing the drying step were presented: stoichiometric relations, kinetic models, diffusion-controlled models and isothermal evaporation processes. Instantaneous evaporation of 10% of the initial water contained in the MSW was assumed during the drying step. For the pyrolysis step, two approaches to model the mass loss were presented, that is kinetics models and pyrolysis fraction (f_p). The latter was chosen. To predict the distribution of CO, CO₂, H₂, H₂O, CH₄, tar and char, a few methods were presented. To take into account the effects of MSW composition, the devolatilization of MSW described by the breakdown of cellulose, hemicellulose and lignin was chosen. All of the nitrogen (N) and sulfur (S) initially contained in the MSW are assumed to be completely transformed into NH₃ and H₂S during the pyrolysis step. Three approaches were presented to model the oxidation step: stoichiometric conversion, heuristic and kinetic models. The heuristic approach that takes into account a sequence of reactions,

TABLE 9: Composition of feedstocks and gasifier operating conditions for two experimental studies.

	1 (Jayah et al., 2003)	2 (Garcia-Bacaicoa et al., 2008)
Feedstock	Wood	17.4% HDPE 82.6% Wood
Flowrate dry basis (kg/h)	18.6	30.9
Moisture content (%)	14.7	25.0
Solids density (kg/m ³)	330	450
Mean particle size (m)	0.055	0.02
Gasifier diameter (m)	0.9	0.44
Gasifier height (m)	0.3	2.0
Air flowrate (kg/h)	34.6	62.1
Drying zone temperature (K)	373	395
Pyrolysis zone temperature (K)	873	634
Oxydation zone temperature (K)	1273	1365
Reductio zone temperature (K)	1173	1084
Oxydant	Air	Air

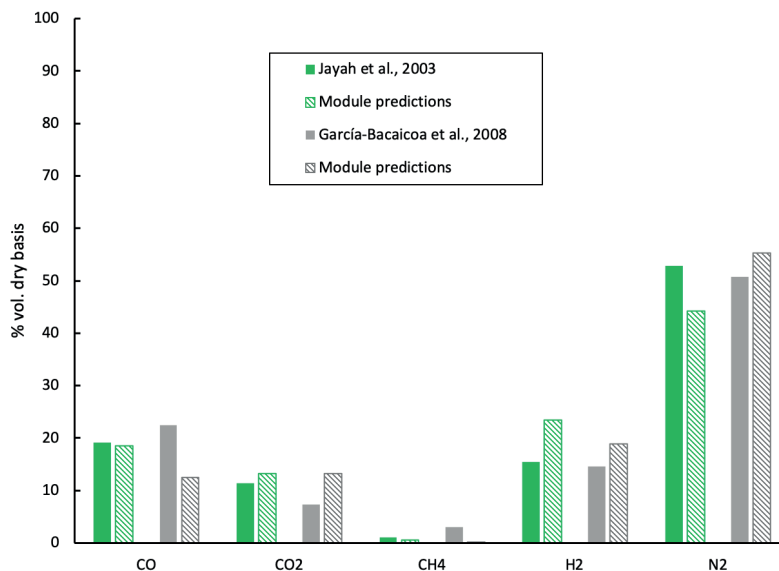


FIGURE 3: Comparisons between the gasification module predictions and experimental results from Jayah et al. (2003) and Garcia-Bacaicoa et al. (2008).

was chosen for this step. Two approaches were presented for the reduction step: the unreacted shrinking core model and the char reactivity factor model. The former model was selected since this model may be applied for both PFR and CSTR reactors, while the latter is specific to PFR only. Finally, the downdraft moving bed reactor was approximated as a PFR, while the fluidized bed reactor was approximated as a CSTR. Water content, MSW composition and average particle size are provided by VMR-Sys as inputs to the gasification module. The module predicts syngas yield, composition and LHV as well as the tar and char contents as functions of the oxidizing agent, operating conditions, reactor types and feedstock composition. The next step will be to integrate this gasification module into VMR-Sys, hence providing a more robust mean of building LCA-inventory data for VMR-Imp.

REFERENCES

Agarwal, G., Liu, G., & Lattimer, B. (2014). Pyrolysis and Oxidation of Cardboard. *Fire Safety Science*, 11, 124–137. <https://doi.org/10.3801/IAFSS.FSS.11-124>

Arena, U. (2012). Process and technological aspects of municipal solid waste gasification. A review. *Waste Management*, 32(4), 625–639. <https://doi.org/10.1016/j.wasman.2011.09.025>

Arena, U., & Di Gregorio, F. (2013). Element partitioning in combustion- and gasification-based waste-to-energy units. *Waste Management*, 33(5), 1142–1150. <https://doi.org/10.1016/j.wasman.2013.01.035>

Babu, B. V., & Sheth, P. N. (2006). Modeling and simulation of reduction zone of downdraft biomass gasifier: Effect of char reactivity factor. *Energy Conversion and Management*, 47(15), 2602–2611. <https://doi.org/10.1016/j.enconman.2005.10.032>

Baillie, R. C., Everett, J. W., Liptak, B. G., Liu, D. H. F., Rugg, F. M., & Switzenbaum, M. S. (1997). Solid waste. In *Environmental Engineers' Handbook* (Second Edition). Boca Raton: CRC Press. Retrieved from <https://www.taylorfrancis.com/books/9781584888598>

Bandara, J., Eikeland, M., & Moldestad, B. M. E. (2017). Analyzing the effects of particle density, size, size distribution and shape for minimum fluidization velocity with Eulerian-Lagrangian CFD simulation (pp. 60–65). Presented at the Proceedings of the 58th Conference on Simulation and Modelling (SIMS 58) Reykjavik, Iceland, September 25th – 27th, 2017. <https://doi.org/10.3384/ecp1713860>

Basu, P. (2010). Gasification Theory and Modeling of Gasifiers. In *Biomass Gasification Design Handbook* (pp. 117–165). Elsevier. <https://doi.org/10.1016/B978-0-12-374988-8.00005-2>

Basu, P. (2013). *Biomass Gasification, Pyrolysis and Torrefaction: Practical Design and Theory*. San Diego, UNITED STATES: Elsevier Science & Technology. Retrieved from <http://ebookcentral.proquest.com/lib/polymtl-ebooks/detail.action?docID=1319046>

Clarke, L. B., & Sloss, L. L. (1992). Trace elements - emissions from coal combustion and gasification. London: IEA Coal Research.

Couhert, C., Commandre, J.-M., & Salvador, S. (2009). Is it possible to predict gas yields of any biomass after rapid pyrolysis at high temperature from its composition in cellulose, hemicellulose and lignin? *Fuel*, 88(3), 408–417. <https://doi.org/10.1016/j.fuel.2008.09.019>

Dejtrakulwong, C., & Patumsawad, S. (2014). Four Zones Modeling of the Downdraft Biomass Gasification Process: Effects of Moisture Content and Air to Fuel Ratio. *Energy Procedia*, 52, 142–149. <https://doi.org/10.1016/j.egypro.2014.07.064>

Di Blasi, C. & Branca, C. (2013). Modeling a stratified downdraft wood gasifier with primary and secondary air entry. *Fuel*, 104, 847–860. <https://doi.org/10.1016/j.fuel.2012.10.014>

Di Blasi, C. (2000). Dynamic behaviour of stratified downdraft gasifiers. *Chemical Engineering Science*, 55(15), 2931–2944. [https://doi.org/10.1016/S0009-2509\(99\)00562-X](https://doi.org/10.1016/S0009-2509(99)00562-X)

Fogler, H. S. (2016). *Elements of chemical reaction engineering*: H. Scott Fogler (Fifth edition). Prentice Hall.

García-Barcaicoa, P., Mastral, J.F., Ceamanos, J., Berruero, C., and Serrano, S. (2008). Gasification of biomass/high density polyethylene mixtures in a downdraft gasifier. *Bioresource Technology*, 99(13), 5485–91. <https://doi.org/10.1016/j.biortech.2007.11.003>

Gerber, S., Behrendt, F., & Oevermann, M. (2010). An Eulerian modeling approach of wood gasification in a bubbling fluidized bed reactor using char as bed material. *Fuel*, 89(10), 2903–2917. <https://doi.org/10.1016/j.fuel.2010.03.034>

Gerber, S., & Oevermann, M. (2014). A two dimensional Euler–Lagrangian model of wood gasification in a charcoal bed – Part I: model description and base scenario. *Fuel*, 115, 385–400. <https://doi.org/10.1016/j.fuel.2013.06.049>

Giltrap, D. L., McKibbin, R., & Barnes, G. R. G. (2003). A steady state model of gas-char reactions in a downdraft biomass gasifier. *Solar Energy*, 74(1), 785–791. [https://doi.org/10.1016/S0038-092X\(03\)00091-4](https://doi.org/10.1016/S0038-092X(03)00091-4)

Grammelis, P., Basinas, P., Malliopoulou, A., & Sakellariopoulos, G. (2009). Pyrolysis kinetics and combustion characteristics of waste recovered fuels. *Fuel*, 88(1), 195–205. <https://doi.org/10.1016/j.fuel.2008.02.002>

- Gupta, S., & Bhaskaran, S. (2018). Numerical Modelling of Fluidized Bed Gasification: An Overview. In S. De, A. K. Agarwal, V. S. Moholkar, & B. Thallada (Eds.), *Coal and Biomass Gasification* (pp. 243–280). Singapore: Springer Singapore. https://doi.org/10.1007/978-981-10-7335-9_10
- Hernández, J. J., Aranda-Almansa, G., & Bula, A. (2010). Gasification of biomass wastes in an entrained flow gasifier: Effect of the particle size and the residence time. *Fuel Processing Technology*, 91(6), 681–692. <https://doi.org/10.1016/j.fuproc.2010.01.018>
- Jafari, R., Sotudeh-Gharebagh, R., & Mostoufi, N. (2004). Modular Simulation of Fluidized Bed Reactors. *Chemical Engineering & Technology*, 27(2), 123–129. <https://doi.org/10.1002/ceat.200401908>
- Jaya, T.H., Aye, L., Fuller, R.J., and Stewart, D.F. (2003). Computer simulation of a downdraft wood gasifier for tea drying. *Biomass and Bioenergy*, 25(4), 459–469. [https://doi.org/10.1016/S0961-9534\(03\)0037-0](https://doi.org/10.1016/S0961-9534(03)0037-0)
- Jung, C.H., Matsuto, T., & Tanaka, N. (2005). Behavior of metals in ash melting and gasification-melting of municipal solid waste (MSW). *Waste Management*, 25(3), 301–310. <https://doi.org/10.1016/j.wasman.2004.08.012>
- Kamińska-Pietrzak, N., & Smoliński, A. (2013). Selected Environmental Aspects of Gasification and Co-Gasification of Various Types of Waste. *Journal of Sustainable Mining*, 12(4), 6–13. <https://doi.org/10.7424/jsm130402>
- Klinghoffer, N., Castaldi, M. J., & Nzihou, A. (2011). Beneficial use of ash and char from biomass gasification. In *Proceedings of the 19th Annual North American Waste-to-Energy Conference NAWTEC19*. Lancaster, Pennsylvania, USA. Retrieved from <http://citeseerx.ist.psu.edu/viewdoc/download?doi=10.1.1.471.6269&rep=rep1&type=pdf>
- Komilis, D. P., & Ham, R. K. (2003). The effect of lignin and sugars to the aerobic decomposition of solid wastes. *Waste Management*, 23(5), 419–423. [https://doi.org/10.1016/S0956-053X\(03\)00062-X](https://doi.org/10.1016/S0956-053X(03)00062-X)
- Levenspiel, O., & Kunii, D. (2012). *Fluidization Engineering* (2nd ed.). Elsevier.
- Liu, H., Elkamel, A., Lohi, A., & Biglari, M. (2013). Computational Fluid Dynamics Modeling of Biomass Gasification in Circulating Fluidized-Bed Reactor Using the Eulerian–Eulerian Approach. *Industrial & Engineering Chemistry Research*, 52(51), 18162–18174. <https://doi.org/10.1021/ie4024148>
- Luo, S., Xiao, B., Guo, X., Hu, Z., Liu, S., & He, M. (2009). Hydrogen-rich gas from catalytic steam gasification of biomass in a fixed bed reactor: Influence of particle size on gasification performance. *International Journal of Hydrogen Energy*, 34(3), 1260–1264. <https://doi.org/10.1016/j.ijhydene.2008.10.088>
- Lv, P. M., Xiong, Z. H., Chang, J., Wu, C. Z., Chen, Y., & Zhu, J. X. (2004). An experimental study on biomass air-steam gasification in a fluidized bed. *Bioresource Technology*, 95(1), 95–101. <https://doi.org/10.1016/j.biortech.2004.02.003>
- Milne T.A., Evans R.J., Abatzoglou N. (1998). Biomass gasifier “tars”: their nature, formation and conversion. National Renewable Energy Laboratory, Golden, CO, report no: NREL/TP-570-25357
- Mostoufi, N., Cui, H., & Chaouki, J. (2001). A Comparison of Two- and Single-Phase Models for Fluidized-Bed Reactors. *Industrial & Engineering Chemistry Research*, 40(23), 5526–5532. <https://doi.org/10.1021/ie010121n>
- Rhodes, M. J. (2008). *Introduction to Particle Technology*. Wiley. Retrieved from <https://ebookcentral.proquest.com/lib/polytml-eb-ooks/detail.action?docID=351230>
- Salem, A. M., & Paul, M. C. (2018). An integrated kinetic model for downdraft gasifier based on a novel approach that optimises the reduction zone of gasifier. *Biomass and Bioenergy*, 109, 172–181. <https://doi.org/10.1016/j.biombioe.2017.12.030>
- Sharma, A.K. (2011). Modeling and simulation of a downdraft biomass gasifier 1. Model development and validation. *Energy Conversion and Management*, 52(2), 1386–1396. <https://doi.org/10.1016/j.enconman.2010.10.001>
- Sharma, A.K., Ravi, M. R., & Kohli, S. (2006). Modelling product composition in slow pyrolysis of wood, 13.
- Sheth, P. N., & Babu, B. V. (2006). Kinetic Modeling of the Pyrolysis of Biomass. In *National Conference on Environmental Conservation (NCEC-2006)* (pp. 453–458). Pilani, India.
- Shokri, N., & Or, D. (2011). What determines drying rates at the onset of diffusion controlled stage-2 evaporation from porous media? *Water Resources Research*, 47(9). <https://doi.org/10.1029/2010WR010284>
- Sikarwar, V. S., Zhao, M., Clough, P., Yao, J., Zhong, X., Memon, M. Z. & Fennell, P. S. (2016). An overview of advances in biomass gasification. *Energy & Environmental Science*, 9(10), 2939–2977. <https://doi.org/10.1039/C6EE00935B>
- Sikarwar, V. S., Zhao, M., Fennell, P. S., Shah, N., & Anthony, E. J. (2017). Progress in biofuel production from gasification. *Progress in Energy and Combustion Science*, 61, 189–248. <https://doi.org/10.1016/j.peccs.2017.04.001>
- Tanigaki, N., & Ishida, Y. (2014). Waste Gasification Technology with Direct Melting for Energy and Material Recovery, 14. Retrieved from http://www.vivis.de/phocadownload/Download/2014_wm/2014_wm_365_378_tanigaki.pdf
- Themelis, N. J., Kim, Y. H., & Brady, M. H. (2002). Energy recovery from New York City solid wastes. *Waste Management and Research*, 20(3), 223–233. Retrieved from <https://doi.org/10.1177/0734242X0202000303>
- Thunman, H., Niklasson, F., Johnsson, F., & Leckner, B. (2001). Composition of Volatile Gases and Thermochemical Properties of Wood for Modeling of Fixed or Fluidized Beds. *Energy & Fuels*, 15(6), 1488–1497. <https://doi.org/10.1021/ef010097q>
- Tinaut, F. V., Melgar, A., Pérez, J. F., & Horrillo, A. (2008). Effect of biomass particle size and air superficial velocity on the gasification process in a downdraft fixed bed gasifier. An experimental and modelling study. *Fuel Processing Technology*, 89(11), 1076–1089. <https://doi.org/10.1016/j.fuproc.2008.04.010>
- US department of Energy. (2008). *Municipal Solid Waste (MSW) to Liquid Fuels Synthesis, Volume 1: Availability of Feedstock and Technology*.
- Vejahati, F., Xu, Z., & Gupta, R. (2010). Trace elements in coal: Associations with coal and minerals and their behavior during coal utilization – A review. *Fuel*, 89(4), 904–911. <https://doi.org/10.1016/j.fuel.2009.06.013>
- Wang, X., De la Cruz, F. B., Ximenes, F., & Barlaz, M. A. (2015). Decomposition and carbon storage of selected paper products in laboratory-scale landfills. *Science of The Total Environment*, 532, 70–79. <https://doi.org/10.1016/j.scitotenv.2015.05.132>
- Wilk, V., Aichernig, C., & Hofbauer, H. (2011). Waste Wood Gasification: Distribution of Nitrogen, Sulphur and Chlorine in a Dual Fluidised Bed Steam Gasifier, 9.
- Williams, P. T., & Williams, E. A. (1999). Interaction of Plastics in Mixed-Plastics Pyrolysis. *Energy & Fuels*, 13(1), 188–196. <https://doi.org/10.1021/ef980163x>